Formation of strained interfaces in AlSb/InAs multilayers grown by molecular beam epitaxy for quantum cascade lasers

Julien Nicolaï, Bénédicte Warot-Fonrose, Christophe Gatel, R. Teissier, A. N. Baranov, Cesar Magen, Anne Ponchet

Formation of strained interfaces in AlSb/InAs multilayers grown by MBE for quantum cascade lasers

J. Nicolaï,[1,4] B. Warot-Fonrose,[1,4] C. Gatel,[1,4,a)] R.Teissier,[2] A. N. Baranov,[2] C. Magen,[3,4] and A. Ponchet[1,4]

[1] *CEMES CNRS-UPR 8011, Université de Toulouse, 29 rue Jeanne Marvig, 31055 Toulouse, France*

[2] *IES CNRS-UMR 5214, 34095 Montpellier, France*

[3] *Laboratorio de Microscopías Avanzadas (LMA), Instituto de Nanociencia de Aragón (INA) - ARAID and Departamento de Física de la Materia Condensada, Universidad de Zaragoza, 50018 Zaragoza, Spain*

[4] *Transpyrenean Associated Laboratory for Electron Microscopy (TALEM), CEMES-INA, CNRS-Universidad de Zaragoza.*

Abstract

Structural and chemical properties of InAs/AlSb interfaces have been studied by transmission electron microscopy. InAs/AlSb multilayers were grown by molecular beam epitaxy with different growth sequences at interfaces. The out-of-plane strain, determined using high resolution microscopy and geometrical phase analysis, has been related to the chemical composition of the interfaces analyzed by High Angle Annular Dark Field imaging. Considering the local strain and chemistry, we estimated the interface composition and discussed the mechanisms of interface formation for the different growth sequences. In particular, we found that the formation of the tensile AlAs-type interface is spontaneously favored due to its high thermal stability compared to the InSb-type interface. We also showed that the interface composition could be tuned using an appropriate growth sequence.

PACS numbers: 68.60.Bs , 68.37.Lp , 68.35.Ct , 68.65.Fg

[a)] Corresponding author : christophe.gatel@cemes.fr

I. INTRODUCTION

The elastic strain is a key parameter of epitaxial heterostructures like those developed for quantum wells. The epitaxial strain results from the elastic accommodation of the lattice misfit between two materials, for instance the substrate and the deposited layer. Many studies have been devoted to probe this strain, but they are generally focused on determining the strain inside nanometric layers. However, the strain variation at interfaces themselves is more complex. Strong strain gradients can occur at interfaces because of chemical exchange over several atomic planes. In addition, the juxtaposition of two materials without common atomic species require chemical bonds at interfaces different from those existing in the two materials. In some cases, these interfaces can undergo a larger distortion than the layers themselves.

This situation is not the most frequent in the epitaxy of III-V compounds, where the simultaneous change of group III and group V elements is often avoided, but it is not fictitious. Indeed, the alternation of wells and barriers without common atoms can provide a great benefit for some systems, particularly antimonide-arsenide systems like AlSb/InAs and GaSb/InAs. The AlSb/InAs system alternates a wide band gap material and a small gap material and its presents a very large conduction band discontinuity of 2.1 eV, beneficial for fabrication of short wavelength quantum cascade lasers (QCLs) (Ref. [1-2]). InAs (here the substrate) and AlSb have close lattice parameters, inducing a moderate misfit of 1.3%. As they have no common atoms, the interfaces consist of either Al-As bonds or In-Sb bonds. Interfaces can thus be Al-As type, In-Sb type, or mixed type. The misfit between InAs (the substrate) and AlAs or InSb, as bulk materials, is -6.6% or +6.9%, respectively. Al-As or In-Sb type interfaces themselves can thus present very large local distortions, which can affect the device properties through a loss of structural quality and a modification of the band structure (Ref. [3, 4]). Although this issue has been identified for a long time, very few studies have been done on the strain induced by this lack of common atoms. The same problematic exists in others arsenide/antimonide systems as InAs/GaSb, where a recent study by transmission electron microscopy (TEM) evidenced a tensile GaAs-like interface (Ref. [5]). In-Sb interfacial bonds were also at the origin of morphological instabilities investigated by synchrotron x-ray diffraction (Ref. [6]) and cross-sectional scanning tunneling microscopy (XSTM) (Ref. [7]). The intermixing at InAs/GaSb interfaces was also studied using high angle annular dark field scanning transmission electron microscopy (HAADF-STEM) (Ref. [8-10]) and atom probe tomography (Ref. [11]). In the InAs/AlSb system discussed here, the strain discontinuities at the scale of the interfaces (1 or 2 atomic layers) remain scarcely studied. The structural studies reported to date concern mainly the interfacial

roughness measured using TEM (Ref. [4, 12]), the interfacial intermixing characterized by XSTM (Ref. [12]), or the possible compensation of strain on a GaSb substrate using various growth sequences (X-ray diffraction study) (Ref. [13]). A similar issue exists in some II-VI systems like ZnTe/CdSe where the favored formation of one of the two possible configurations was recently observed by HAADF-STEM (Ref. [14]). This system, however, does not involve strain discontinuities as important as here.

In a recent work (Ref. [15]), we have shown that such interfacial layers are formed in the InAs/AlSb system. The elastic strain induced by the interfaces themselves can be experimentally observed at a very local scale and analyzed qualitatively. In this article, we intend to investigate more deeply the nature of the interfacial bonds in this system by combining two methods of characterization at the scale of the interface. Information on chemical composition and strain is thus analyzed independently, by HAADF-STEM and high resolution TEM (HRTEM) respectively. The combination of chemical and strain data allowed refining the actual composition of interfaces. Then the formation of the interfaces is discussed on the basis of the physical mechanisms involved. As MBE is an out-of-equilibrium process, the interface formation is a sequential process, which depends on the succession of microscopic events that occur at the surface. It is well known that due to this feature, direct and reverse interfaces are generally not equivalent. One of the questions we intend to answer in this context is whether the formation of one of the possible interfacial configurations is favored. For this purpose, a multilayer with very simple interfacial sequences was investigated in order to determine the so-called spontaneous interfaces. In our previous report (Ref. [15]) the predominance of Al-As type interfaces was observed, which can be attributed to the greater stability of AlAs compared with InSb. Here we discuss comparatively the formation of direct and reverse interfaces in InAs/AlSb multilayer structures.

Then, for a better understanding of the interfacial formation mechanism, we have tried to force the two extreme cases, *i.e.* either Al-As or In-Sb type interface. In practice, we have introduced a very short sequence of either AlAs or InSb; the duration of the deposit corresponded to 0.7 monolayer. The analysis of the results should give clear insight about the mechanisms favoring formation of the actual interfaces. In particular, the asymmetry of direct and reverse interfaces can be explained by considering atomistic mechanisms at the growing surface. Forcing the interfaces can furthermore be useful to control electronic properties, which depend not only on the two materials considered separately, but also on the exact atomic configuration of interfaces, especially in QCLs containing ultra-thin layers.

II. EXPERIMENTAL DETAILS

InAs/AlSb multilayers have been grown by molecular beam epitaxy (MBE) at 700 K on (001) InAs substrates at a growth rate of 1 $A.s^{-1}$. Antimony and arsenic valved cracker cells were used and the V/III flux ratio was close to 2 for both the InAs and AlSb layers. Their thicknesses, respectively 20 nm and 4 nm, are larger than in QCLs in order to avoid superposition of fields of displacement from adjacent interfaces. These values appear as a suitable compromise to meet this objective without risk of plastic relaxation. The growth sequences are described in Fig. 1. In sample A, the interfaces are spontaneously self-assembled while in sample B and C we tried to control the interfaces formation by the insertion of very small amounts of either AlAs or InSb corresponding to a deposit of 2/3 of a full monolayer. In sample B we intended to force Al-As type bonding at the first interface (before the deposition of AlSb on the InAs) and In-Sb type bonding at the second interface (before the deposition of InAs on the AlSb). This sequence is reversed in sample C. At all interfaces, growth interruptions without any flux were employed to avoid mixing of the group V elements.

For TEM experiments, cross-sectional specimens have been prepared by mechanical polishing and argon ion milling at low temperature using a Gatan Precision Ion Polishing System equipped with a liquid nitrogen cooling system. For each sample, several specimens were thinned along both [1-10] and [110] zone axes (which can present different interfacial step structures). The samples have been observed by HRTEM on a TECNAI F-20 operating at 200 kV, equipped with a spherical aberration corrector for the objective lens to avoid the delocalization effect at interfaces and to achieve a 0.12 nm resolution. Images have been realized on a 2k x2k CCD camera, in white-atoms conditions using the negative spherical aberration imaging method with a C_s close to -1µm (Ref. [16]).

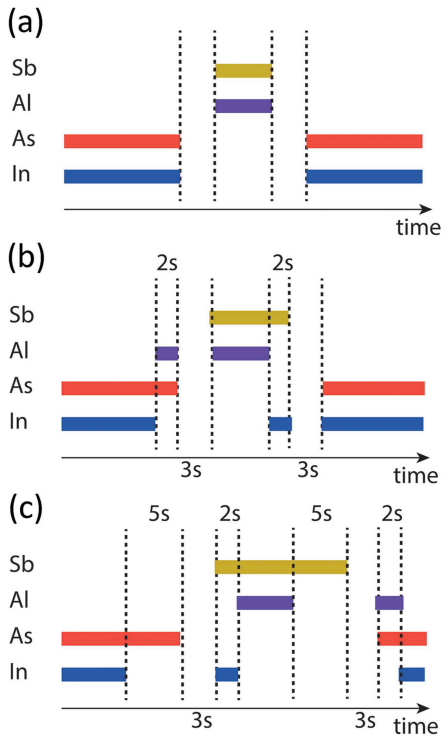

FIG. 1. (Color on line) Growth sequence of the samples. (a) In the sample A the interfaces are spontaneously assembled. (b) In the sample B we tried to make AlAs then InSb interfaces while in the sample C (c) we tried to make InSb then AlAs interfaces.

The strain state of the samples has been determined using the geometrical phase analysis (GPA) method (Ref. [17])**.** We used two vectors of the reciprocal lattice $\mathbf{g_1}$ and $\mathbf{g_2}$ (**[220]** and **[002]**) to determine the 2D displacement field **u(r)** of the atomic planes. A cosine mask has been used in the reciprocal space allowing a 0.8 nm space resolution in the direct space. For each resulting phase image, a reference zone of 4x20 nm² has been chosen in the middle of one InAs layer after correcting numerically the distortion induced by the camera. The strain field components have been determined by the well-known relationship:

$$\varepsilon_{ij} = \frac{1}{2}\left(\frac{\delta u_i}{\delta x_j} + \frac{\delta u_j}{\delta x_i}\right) \quad (1)$$

Strain profiles in the growth direction have been extracted from strain maps, after averaging on 30 nm in the direction parallel to the interfaces. For each sample, the strain fields did not exhibit any significant difference due to the choice of the [1-10] or [110] zone axis.

HAADF-STEM imaging has been performed on a TITAN 60-300 operated at 300 kV and equipped with a high-brightness field emission gun (X-FEG), a Wien filter monochromator and a probe aberration corrector reaching a spatial resolution of 0.08 nm in STEM. In HAADF-STEM mode, the intensity scattered by each atomic column increases with the average atomic number Z (Ref. [18, 19]). Simulations, using the QSTEM package (Ref. [20]) were made to ensure that the intensity in the image is proportional to Z^n, with n close to 1.7 for the 4 elements considered in this study. Note that the GPA method cannot be applied to these STEM-HAADF images. Indeed, to reduce the artifacts due to the scanning process it is necessary to realize two images rotated of 90 degrees of the same area, which was not possible here due to the fragility of the sample under electronic beam.

III. PRINCIPLES OF THE INTERFACIAL ANALYSIS

A. Nature of interfaces

We can distinguish three types of interfaces to which we refer as minimal, topological and chemical (cf. Fig. 2). The minimal interface between the InAs and AlSb layers consists of the necessary atomic bonds, Al-As or In-Sb, due to the fact that AlSb and InAs have no common atoms. The width of the so-called minimal interface is one atomic bond (cf. Fig. 2(a)). Moreover, in the semiconductor materials, the interfacial roughness (presence of steps of one or more monolayers) induces a topological interface (cf. Fig. 2(b)). Finally, in the case of miscible materials as here, the diffusion or exchange mechanisms result in the formation of a mixed interface. This phenomenon, which can occur on several monolayers, can then be predominantly responsible for the nature and the width of the interface (cf. Fig. 2(c)). This interface corresponds to the chemical interface. Due to the fact that the TEM/STEM image is a projection through the electron path, it is not possible to differentiate the chemical interface and the topological interface, if the thickness of thinned foil is larger than the size of the terraces.

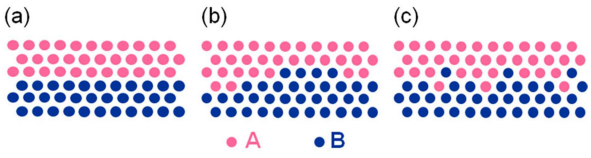

FIG. 2. (Color on line) Schematic representation of the different types of interface between two systems, A and B, with no common atoms. (a) Minimal interface with a simple atomic bond between A and B layers. (b) Topological interface due to roughness, generally about one atomic layer in the semiconductor materials. (c) Chemical interface where the diffusion mechanisms (for miscible materials) result in an intermediate mixed layer.

B. Strain analysis

The misfit *f* can be defined as:

$$f = \frac{\alpha_f - \alpha_s}{a_s} \quad (2)$$

where a_s and a_f are the bulk lattice parameters of the substrate and the film, respectively. In the case where $a_f < a_s$, the layer is stressed in tension while if $a_f > a_s$ it is in compression. Considering epitaxial growth of cubic cells along the [001] direction, in the framework of linear elasticity, the in-plane and out-of-plane components of the strain, $\varepsilon_{//}^{abs}$ and $\varepsilon_{\perp}^{abs}$ respectively, are theoretically given by:

$$\varepsilon_{//}^{abs} = -f \quad \text{and} \quad \varepsilon_{\perp}^{abs} = -2\left(\frac{C_{12}}{C_{11}}\right)\varepsilon_{//}^{abs} = 2\left(\frac{C_{12}}{C_{11}}\right)f \quad (3)$$

where C_{11} and C_{12} are the elastic constants of the layers (Table I).

TABLE I. Lattice parameters and elastic constants of the binary bulk compounds (data from ref. [21]).

	a_f (nm)	C_{11} (GPa)	C_{12} (GPa)	$1+2\left(\frac{C_{12}}{C_{11}}\right)$
AlAs	0.5660	125.48	53.54	1.85
AlSb	0.6136	87.80	43.51	1.99
InAs	0.60583	83.32	45.30	2.09
InSb	0.64794	66.65	36.41	2.09

As the size of an interface and the high strains are outside the usual range of validity of linear elasticity, we also performed an atomistic modeling based on the first principles density functional theory (DFT) (see for instance ref. [22]). Although the linearity of the stress-strain relationship fails, we found that the out-of-plane strain of a single AlAs (or InSb) atomic layer forming an interface between InAs and AlSb is in good agreement with (3), using the elastic constants calculated by DFT for bulk materials. This allows us to link the out-of-plane strain with the lattice misfit through (3) even in case of ultra-thin interfaces and lattice mismatch as important as -6.6% (or +6.9%).

As with GPA the displacements of the atomic planes are measured comparatively to a reference zone chosen in the middle of an InAs layer (supposed to be strain free), the in-plane and out-of-plane strains $\varepsilon_{//}$ and $\varepsilon_{\perp}$ measured

from (1) are relative to the substrate, that is to say that they are related to the absolute strain components $\varepsilon_{//}^{abs}$ and $\varepsilon_{\perp}^{abs}$ by

$$\varepsilon_{//} = \varepsilon_{//}^{abs} + f \quad and \quad \varepsilon_{\perp} = \varepsilon_{\perp}^{abs} + f \ .$$

In case of a fully strained layer it comes from (3):

$$\varepsilon_{//} = 0 \quad and \quad \varepsilon_{\perp} = f\left[1 + 2\frac{C_{12}}{C_{11}}\right]. \qquad (4)$$

Through (4), information on chemical composition can thus be inferred from the out-of-plane strain analysis performed on HREM images. Fig. 3(a) shows f, the misfit with InAs calculated using (2), for the four possible ternary compounds (the lattice parameters of alloys being deduced from the binaries using the Vegard's law). As shown by this graph, $In(As_{1-y},Sb_y)$ (red curve) and $(Al_{1-x},In_x)Sb$ (green curve) compounds are stressed in compression ($f>0$), while $(Al_{1-x},In_x)As$ (blue curve) is stressed in tension ($f<0$). The $Al(As_{1-y},Sb_y)$ (black curve) compound can be in tension (if $y \leq 0.84$) or in compression (if $y \geq 0.84$). For AlInAsSb quaternary alloy, one given strain value corresponds to several compounds as shown by the iso-misfit curves displayed Fig. 4(a).

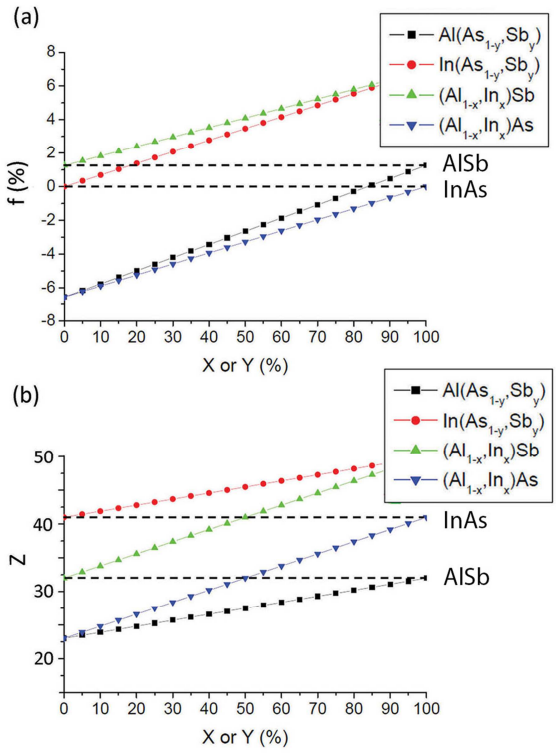

FIG. 3. (Color on line) (a) Misfit f with InAs and (b) average atomic number Z, for the four possible ternary compounds. The horizontal dashed lines correspond to InAs and AlSb.

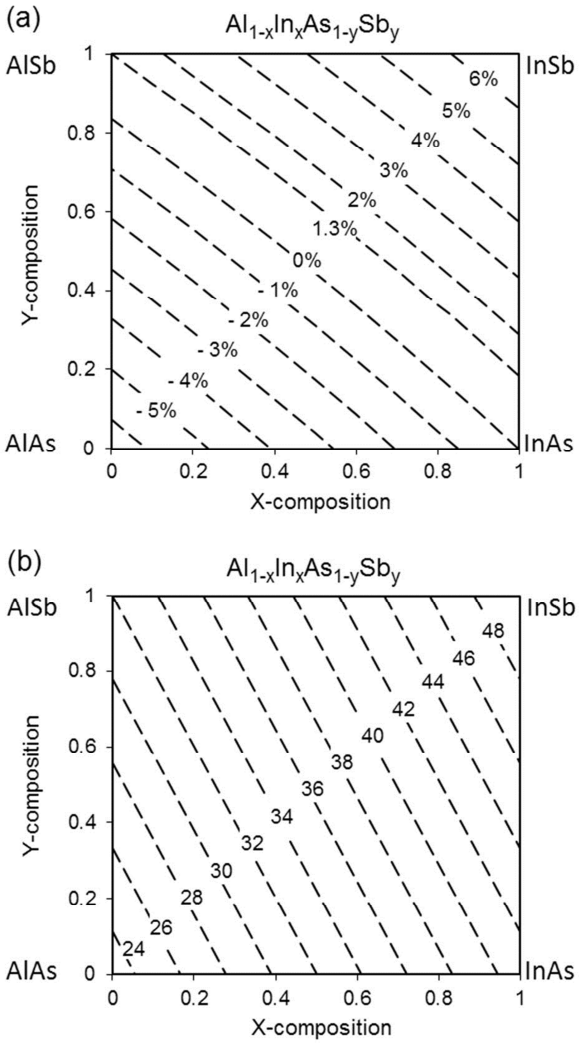

FIG. 4. Curves of (a) iso misfit with InAs substrate and (b) iso average Z versus chemical composition, for quaternary alloys.

The determination of the exact value of the interfacial strain is difficult at the scale of an interface. Indeed, two kinds of phenomena have to be considered: growth effects and image analysis effects. Concerning the first point, the atomic steps (Fig. 2(b)) and the local variation of chemical composition (Fig. 2(c)) cannot be avoided causing three dimensional inhomogeneities in the sample. The composition is thus averaged across the electron path. Concerning the second point, the strain value obtained by the GPA method in HRTEM depends on the imaging conditions, such as focus (Ref. [23]), and requires a perfect homogeneity of the image. In practice, thickness fluctuations and/or dynamical effects induce a local change of imaging conditions, especially at the interfaces. The use of a spherical aberration corrector suppresses delocalization effects at the interfaces, which is critical for the GPA analysis.

Moreover, the spatial resolution of the GPA treatment is limited by the size of the mask used in the reciprocal space. Here, this spatial resolution is 0.8 nm, i.e. larger than the interface width or of the same order of magnitude. This implies a reduction of the measured strain compared to the actual one, and a widening of the profile. For these reasons, the precise values of strain in the vicinity of interfaces cannot be found and only semi-quantitative information can be obtained. In practice, we will thus determine a range of composition compatible with the experimental data, keeping in mind that the measured strain is most likely attenuated compared to the actual strain.

C. Composition analysis

HAADF-STEM images are analyzed with a quite similar qualitative approach. They are used to obtain chemical information by comparing the intensity scattered by the interfaces with I^{HAADF}_{AlSb} and I^{HAADF}_{InAs}, the intensities diffused by InAs and AlSb layers, respectively. As well as for the strain, several compositions correspond to one particular value of diffused intensity, as shown in Fig.3(b) for the ternary compounds and Fig.4(b) for the AlInAsSb alloys. Fig.4(b) can be easily divided into three parts: first: intensity lower than I^{HAADF}_{AlSb} (compounds lighter than AlSb); second: intensity greater than I^{HAADF}_{InAs} (compounds heavier than InAs); third: intensity between I^{HAADF}_{AlSb} and I^{HAADF}_{InAs} (compounds with an intermediate Z). By restricting this analysis to ternary compounds (Fig.3(b)), these three parts are defined by: first: Al(As,Sb) or $(Al_{1-x},In_x)As$ with $x \leq 0.5$ (lighter composition than AlSb); second: In(As,Sb) or $(Al_{1-x},In_x)Sb$ with $x \geq 0.5$ (heavier composition than InAs) ; third: $(Al_{1-x},In_x)Sb$ with $x \leq 0.5$ or $(Al_{1-}x,In_x)As$ with $x \geq 0.5$ (intermediate between InAs and AlSb).

By coupling the GPA and HAADF results it is thus expected to go further in the estimation of the possible compositions of the interfaces than by using only one method.

IV. RESULTS

As described in the previous section, the strain and chemical profiles can be qualitatively analyzed by considering all possible alloys. Figure 5(a) shows an HRTEM image of the sample A along the [110] zone axis. It shows the very good quality of the epitaxy without any plastic relaxation; a very weak contrast indicates the presence of the 4 nm thick AlSb layer between two InAs layers. The map of the in-plane strain $\varepsilon_{//}$ is homogeneous and it is close to zero. The $\varepsilon_{\perp}$ mapping in Fig. 5(b) clearly shows a layer in compression (the yellow part with 4 nm

in width) surrounded by two symmetrical layers in tension (in blue). The out-of-plane strain profile $\varepsilon_{\perp}$ exhibits three different strain states, two sharp and negative peaks (respectively -1 and -2%) and a plateau around 2.2% (Fig. 5(c)). To ensure reproducibility of these results, several HRTEM observations have been performed on sample A. Moreover, these observations have been realized in the two <110> directions of the (001) plane and the corresponding profiles are qualitatively similar. The different values obtained for the plateau are comprised between 2% and 3%. These results are compared with the theoretical value assuming that AlSb is fully strained. From equation (4), with C_{11} and C_{12} of respectively 87.8 GPa and 43.5 GPa (Ref. [21]) we obtain 2.3%, a value that has to be corrected by 10 to 20% due to the thin foil effect (Ref. [24]). The expected value is thus close to 2.1%. Experimental values are thus in good agreement and confirm that the AlSb layer is fully strained. The fact that the measured strain $\varepsilon_{\perp}$ can be slightly larger than expected suggests a possible incorporation of a small amount of indium due to segregation (Ref. [25]).

With an out-of-plane measured strain of -1 and -2%, the interfaces can be described as being under a moderate tensile stress. From Fig. 5(c) and considering the interpretation based on Fig. 4(a), the two negatives peaks can be attributed to $(Al_{1-x},In_x)As$ or $Al(As_{1-y},Sb_y)$ ($y \leq 0.84$), or quaternaries between AlAs, InAs and $AlAs_{0.16}Sb_{0.84}$.

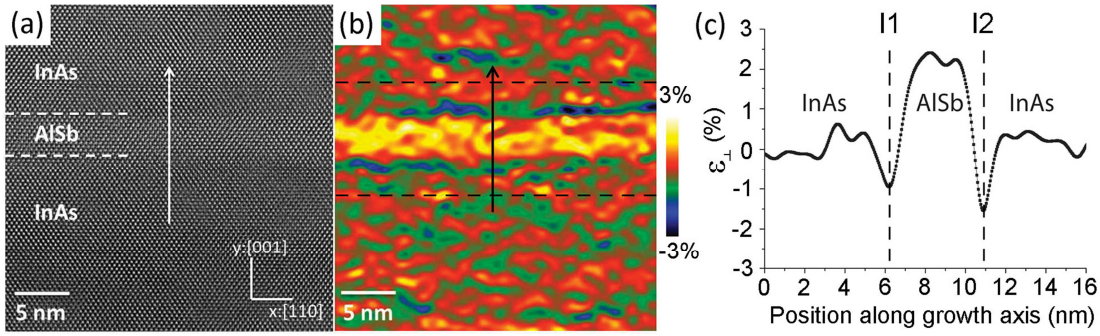

FIG. 5. (Color on line) (a) HRTEM image of A sample [110] zone axis, (b) $\varepsilon_{\perp}$ mapping, (c) $\varepsilon_{\perp}$ strain profile obtain by GPA averaged on the whole width of the image (30 nm). The white arrow indicates the growth direction.

Figure 6 presents an HAADF-STEM image of the same sample, along the [110] zone axis. This image exhibits three different intensities corresponding to the InAs layer (the brightest layer on the image), the AlSb layer (darker than InAs) surrounded by two very thin layers with an intensity lower than AlSb (the darkest layers). From Fig. 4(b), it is possible to determine that the interfaces (the darkest layers) are lighter than InAs and AlSb layers. The

corresponding compounds are the ternaries (Al,In)As with the In composition less than 50%, Al(As,Sb) and by extension the quaternaries between AlAs, AlSb and $Al_{0.5}In_{0.5}As$.

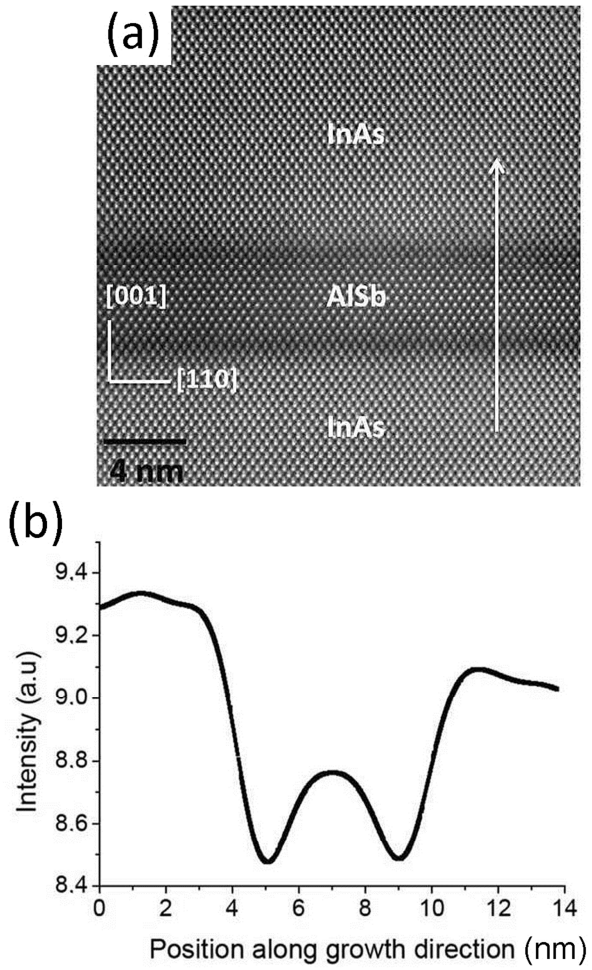

FIG. 6. (a) HAADF-STEM micrograph of sample A. The arrow indicates the growth direction. (b) Intensity profile of HAADF micrography, plotted along the growth direction. The intensity is given in arbitrary unit (the intensity variation between the different InAs layers is related to the thickness variation of the sample).

By coupling the results obtained by HRTEM and HAADF-STEM, the composition of the interfaces of the sample A can be identified as $(Al_{1-x},In_x)As$ ($x \leq 0.5$) or $Al(As_{1-y},Sb_y)$ ($y \leq 0.85$) or any quaternary in the quadrangle limited by AlAs, $Al_{0.5}In_{0.5}As$, $AlAs_{0.16}Sb_{0.84}$ and $Al_{0.87}In_{0.13}As_{0.26}Sb_{0.74}$ (labelled 1 in fig.7). Although the exact composition of the interfaces cannot be given from this analysis, it appears clearly that the interfaces exhibit an Al rich character.

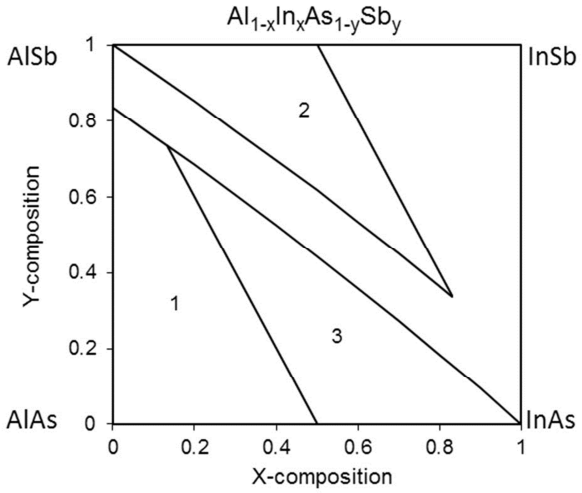

FIG. 7. Quaternary compounds composition from HRTEM and HAADF-STEM analysis.

The in-plane strain profiles of samples B and C are similar to sample A, proving their high epitaxial quality. The out-of-plane strain profiles for samples B and C show three different strain states, two peaks corresponding to the interfaces and one plateau around 2 to 2.5%. As for sample A this plateau can be attributed to the AlSb layer. In the following, the interface will be named first (I1) or second (I2) interface, according to the growth sequence, *i.e* AlSb grown on AlSb or InAs grown on AlSb, respectively.

The sample B presents two strongly asymmetric interfaces, the first in tension and the second in high compression. In the Fig. 8(a and b) the measured out-of-plane strains are -4% (I1) and +4% (I2). Depending on the area and/or the thinned specimen, these values can reach -7% and +7% respectively. The first interface is thus attributed to the ternaries and the quaternaries limited by AlAs, InAs and $AlAs_{0.16}Sb_{0.84}$. Concerning the second interface, the compounds with a larger misfit than AlSb are the ternaries and quaternaries limited by AlSb, InSb, and $InAs_{0.82}Sb_{0.18}$. The HAADF-STEM analysis (Fig. 8(c) and 8(d)) indicates that the first interface is lighter than AlSb, which can correspond to $(Al_{1-x},In_x)As$ ($x \leq 0.5$) or $Al(As_{1-y},Sb_y)$ or the quaternaries between AlAs, AlSb and $Al_{0.5}In_{0.5}As$. The second interface appears to be heavier than the AlSb layer and lighter than the InAs layer, which can be attributed to the presence of $(Al_{1-x},In_x)As$ ($x \geq 0.5$) or $(Al_{1-x},In_x)Sb$ ($x \leq 0.5$) or quaternaries limited by

$Al_{0.5}In_{0.5}As$, InAs, $Al_{0.5}In_{0.5}Sb$ and AlSb. Combining these results, we deduced that the first interface consists of $(Al_{1-x},In_x)As$ ($x \leq 0.5$) or $Al(As_{1-y},Sb_y)$ ($y \leq 0.84$), or any quaternary in the quadrangle limited by AlAs, $Al_{0.5}In_{0.5}As$, $Al_{0.87}In_{0.13}As_{0.26}Sb_{0.74}$ and $AlAs_{0.16}Sb_{0.84}$ (labelled 1 in Fig. 7). Moreover, the high level of strain (-4 to -7%) allows us to consider that its composition is closer to AlAs than to others limits. The second interface can only correspond to the compounds in the triangle limited by AlSb, $Al_{0.5}In_{0.5}Sb$ and $Al_{0.17}In_{0.83}As_{0.66}Sb_{0.34}$ (labelled 2 in Fig.7). The high value of the measured strain (4 to 7 %) makes possible a reduction of this range toward a composition close to $Al_{0.5}In_{0.5}Sb$. Interfaces are therefore AlAs rich and $Al_{0.5}In_{0.5}Sb$ rich, respectively.

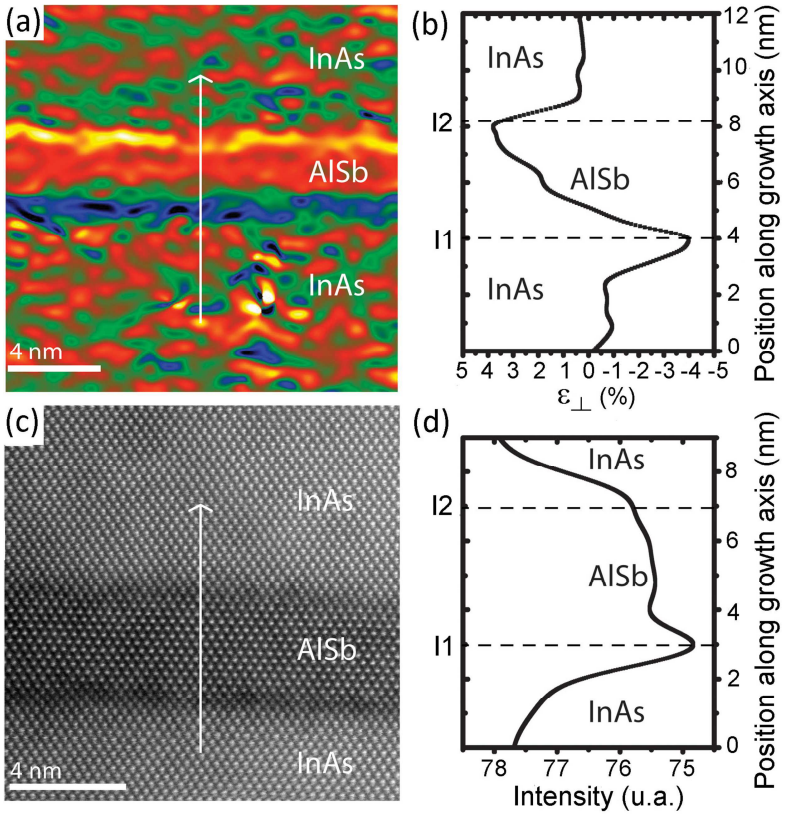

FIG. 8. (Color on line) (a) $\varepsilon_\perp$ mapping of B sample, from GPA of an [110] zone axis HRTEM image, (b) $\varepsilon_\perp$ strain profile averaged on the whole width of the image (30 nm), (c) HAADF-STEM micrograph of sample B, (d) Intensity profile of this HAADF micrography plotted along the growth direction.

Strain profile obtained for the sample C in Fig. 9(a) and 9(b) shows that the interfaces are moderately stressed in tension with respectively $\varepsilon_\perp$ = -1% and -2%. These interfaces could correspond to ternaries or quaternaries limited by AlAs, InAs and $AlAs_{0.14}Sb_{0.86}$. The obtained HAADF-STEM profile (Fig.9(c) and

9(d)) exhibits an asymmetric shape : the first interface is brighter than the AlSb layer and darker than InAs layer, while the second interface is significantly darker than the AlSb layer. Considering these results, the first interface consists of ternaries or quaternaries limited by $Al_{0.5}In_{0.5}As$, InAs, $Al_{0.5}In_{0.5}Sb$ and AlSb while the second interface corresponds to compounds limited by AlAs, AlSb and $Al_{0.5}In_{0.5}As$. By combining HRTEM and HAADF, for the first interface this range is restricted to the triangle $Al_{0.5}In_{0.5}As$, InAs and $Al_{0.87}In_{0.13}As_{0.26}Sb_{0.74}$ (labelled 3 in Fig.7). *The moderate but significant* strain suggests a composition closer to $Al_{0.5}In_{0.5}As$ than to other limits. For the second interface, this range is restricted to the quadrangle AlAs, $Al_{0.5}In_{0.5}As$, $Al_{0.87}In_{0.13}As_{0.26}Sb_{0.74}$ and $AlAs_{0.16}Sb_{0.84}$ (labelled 1 in Fig.7) i.e. the interface exhibits a rich Al character.

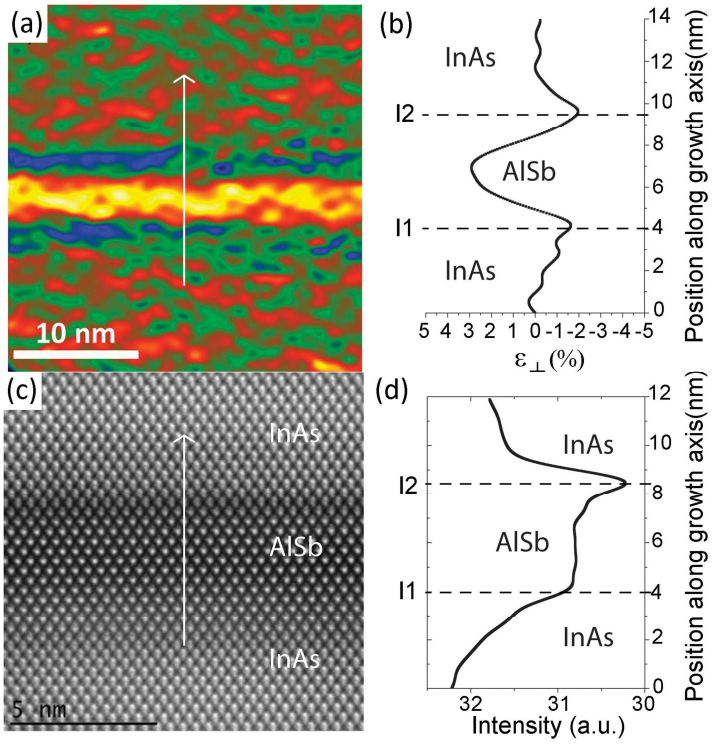

FIG. 9. (Color on line) (a) $\boldsymbol{\varepsilon_{\perp}}$ mapping of C sample, from GPA analysis of an [110] zone axis HREM image, (b) $\boldsymbol{\varepsilon_{\perp}}$ strain profile averaged on the whole width of the image (30 nm), (c) HAADF-STEM micrograph of sample C, (d) Intensity profile of the HAADF micrography, plotted along the growth direction.

V. DISCUSSION

A. Mechanisms

As AlSb and InAs have no common atoms, the chemical bonds at interfaces are not defined a priori. First, the minimal interface (as defined in Fig. 2(a)) is affected by the employed growth sequence. Then, the formation of the actual interfaces results from the competition between different mechanisms. The bulk binaries corresponding to the four possible chemical bonds existing in this system present very different melting points and cohesive energies (Table II, data from Ref. [21]). The two binaries corresponding to the candidates to form the interfacial bonds, AlAs and InSb, are respectively the more stable and the less stable among the four compounds. The Al-As type interface appears as a much more stable interface than In-Sb type. Unlike the binary compounds, ternary and quaternary alloys are generally not thermodynamically stable in the whole range of compositions, but present a gap of miscibility depending on the temperature of their formation (Ref. [26, 27]). Regarding AlInAsSb, the calculations suggest a large gap at 723 K (Ref. [28]). Purely thermodynamic considerations are obviously not sufficient. The epitaxial growth is an out-of-equilibrium process that allows the growth of metastable compositions, reducing the miscibility gap (Ref. [29]).

TABLE II. Physical properties of the binary bulk compounds (Data from ref. [21]).

Crystal	Melting Point (K)	Cohesive energy (eV)
AlAs	2013	6.8
AlSb	1338	6.6
InAs	1215	5.4
InSb	800	4.7

In MBE growth, it is known that direct and reverse interfaces are not equivalent because of the competition between various elementary processes at the growing surface, such as incorporation, desorption, and exchange. This is particularly important in III-V compounds which are miscible and can form alloys. The probability that these elementary mechanisms occur is different for atoms of group III and group V, and for the different chemical species inside one group. At the growth temperature of 723K and in regular growth conditions, *i.e.* under an excess of group V flux compared to group III flux, both Al and In have a sticking coefficient close to 1, which means that all Al and

In deposited atoms participate in the growth. Nevertheless, segregation of indium versus other III atoms is a well-known phenomenon, which has been widely studied in the GaInAs system **(**Ref. [29-31]). Here, it is thus reasonable to consider that the exchange of an incoming Al atom with an In atom already incorporated is possible, while the reverse situation is much less likely (Al being much more strongly bonded with the atom of group V than In). The situation is different for atoms of group V, which are in excess and can desorb in the vapor phase. For these reasons, direct and reverse interfaces do not obey the same scheme of formation.

In this section the formation of the two interfaces (AlSb on InAs then InAs on AlSb) will thus be discussed separately. For each of them we will first discuss the possible mechanisms of formation of the so-called "spontaneous" interface, then we will consider the formation of interface when a short sequence of either Al-As or In-Sb is intentionally introduced. For each configuration, after determining the minimal interface from the growth sequence, the formation of a chemical interface due to exchanges will be discussed. A possible scheme of formation, based on the physical mechanisms mentioned above, will be proposed and compared to the experimental data. The atomic layers likely to exchange their position in the stacking sequence will be labelled and written in bold. At each step, exchanges will be considered only between the two last layers.

B. Formation of I1 interface (AlSb on InAs)

The growth sequence of the sample A did not intend to promote a specific type of interface and leads to the spontaneous formation of interfaces. The expected atomic stacking is thus of the type In-As-$\mathbf{In_1}$-As-$\mathbf{Al_1}$-Sb *i.e.* the minimal interface is a single plane of Al-As bonds. As it is a very stable bond (the most stable amongst the four possible), it can thus be easily formed. Arsenic desorption and its substitution by Sb is unlikely. Nevertheless, due to the segregation of In respectively to Al, $\mathbf{In_1}$ can exchange its position with the $\mathbf{Al_1}$ leading to the formation of (Al,In)As rich interface rather than a pure AlAs one. This scenario is very consistent with our experimental analyses. Incorporation of the segregated In atoms into the AlSb layer can explain the higher value of strain than expected which is sometimes observed.

The growth sequence in sample B was expected to provide the In-As-In-$\mathbf{As_1}$-$\mathbf{Al_1}$-$\mathbf{As_2}$-$\mathbf{Al_2}$-Sb succession of atomic bonds at the first interface. An AlAs layer has been added compared with the sample A to strengthen the Al-As character of the minimal interface, which is thus three successive Al-As bonds. By this way the tensile stress at the first interface should be larger than in the sample A. Experimentally, we observed that the strain measured at the

first interface of the sample B (-4% to -7%) is much higher than in sample A (close to -1%) and that this interface has a clear Al-As character, which is in a very good agreement with our interface formation model.

In sample C we tried to make a minimal interface of the In-Sb type on an InAs surface saturated with As. Considering the growth sequence we can write the nominal alternation of bonds as In-As-**In_1**-**Sb_1**-**Al_1**-Sb. For a given III element, III-As bonds being more stable than III-Sb ones, As terminating the InAs surface cannot switch its position with Sb. On the contrary, during the co-deposition of In and Sb on InAs (As rich) surface, while the group III element cannot easily desorb at this growth temperature (Ref. [32]) and is fully incorporated, Sb_1 can be replaced by As in excess on the InAs surface. Then, during the deposition of AlSb, the **In_1** can partially exchange with the **Al_1**, leading to the formation of an (Al,In)As rich interface in case of full desorption of **Sb_1**, or to a more complex quaternary composition if only a part of **Sb_1** has desorbed. This result is in a very good agreement with results obtained by microscopy, which showed that the In-Sb interface configuration cannot be achieved using this growth sequence (the observed interface is wide and slightly in tension).

C. Formation of I2 interface (InAs on AlSb)

Now consider the second interface of the three samples described above. In the sample A, the second interface consists nominally of the Al-**Sb_1**-In-**As_1**-In-As sequence, *i.e.* the minimal interface is one plane of In-Sb bonds. In this sequence, exchange of group III elements is unlikely. But we can assume that the Sb_1 can easily desorb and be replaced by As_1 (deposited in excess). This scenario, favored by the unstable character of the In-Sb bond, would lead to the formation of one plane of Al-As, the most stable atomic bond, if this exchange is complete, or to a mixed Al-(As,Sb)-In interface extending over at least 2 planes, in case of uncompleted exchange. Note that the Sb atoms that have been replaced by As atoms are not necessarily incorporated later on, but can also fully desorb. Results obtained by our image analysis showed the formation of an Al rich interface in tension, which is fully consistent with these hypotheses based on the growth sequence.

In sample B the intentional formation of In-Sb interface was tested using the following sequence: Al-**Sb_1**-**In_1**-**Sb_2**-In-**As_1**, *i.e.* 3 successive In-Sb bonds. With the same hypotheses as in the previous case, exchange of group III elements is unlikely but replacement of Sb_2 by As_1 is possible. We indeed assume that during the growth interruption the Sb_2 can easily desorb and be replaced by As. If this concerns only the last Sb plane, the In-Sb character of the interface should be preserved. Our TEM analyses suggest a rich Sb interface with however a mixed

composition of the group III elements. This can be explained by a more complex exchange process probably related to the unstable character of the InSb bond.

In the sample C, we tried to form a minimal interface of the Al-As type with the sequence Al-**Sb**$_1$-Al-**As**$_1$-In-As. While exchange of group III elements is not likely, an exchange between Sb1 and As1 can occur leading to a wider interface, extending over at least three successive bonds of either AlAs (in case of full desorption of Sb) or Al(As,Sb). The results of the HRTEM and HAADF-STEM analyses are in a good agreement with the expected composition of the interfaces, *i.e* Al-rich interface with a tensile stress.

VI. CONCLUSION

The interface strain state has been studied by HRTEM analysis using the GPA method. This strain state can be related to the chemical composition of the interfaces themselves. Due to the technical limitations of the method (spatial resolution, choice of the reference zone…) and to the averaging effects in the direction of observation, the strain value at the scale of an interface cannot be measured as precisely as in thicker layers. In particular, the actual strain is probably larger than the measured one**.** Finally, translate strain data into chemical data in a quaternary system does not lead to a unique solution. Therefore, only semi-quantitative information can be deduced like AlAs-rich (tensile stress) or InSb-rich (compressive stress) interfaces. The chemical composition of these interfaces has also been investigated by HAADF-STEM. Similarly, several chemical compositions can account for one HAADF intensity profile. The combination of these two techniques allows a more precise description of the interface composition.

In parallel, examining the growth sequence and using only a limited number of hypotheses, we determine the possible chemical composition of the interfaces. These assumptions are: (i) the elements of group V can desorb while those of group III cannot, (ii) exchanges are possible between In and Al, due to In segregation versus Al, and (iii) between Sb and As leading to a better incorporation of As than Sb. Moreover, we assume (iv) that the more the bonding is strong, the more it is favored. The use of these rules leads to the determination of the chemical composition of the interfaces in a very good agreement with the experimental results.

We showed that spontaneously, without any special flux conditions, Al-As bonds are favored on both AlSb on InAs interfaces and InAs on AlSb interfaces. We assume that the Al-As type interface is favored due to its high

thermal stability and bond energy. It should be noted that, in the case of sample A, although strain and Z-contrast profiles are comparable for the first and the second interfaces, the growth sequence analysis suggests different compositions. Indeed, the possible exchange between III elements at the first interface leads to an alloy close to (Al,In)As, while the possible mixing of V elements lead to a more complex alloy (Al,In)(As,Sb) at the second interface. Further experiments are underway to investigate this point.

Then, the intentional insertion of either an AlAs or InSb sequence gave a clear insight about the mechanisms favoring the formation of these interfaces. Indeed, the intentional addition of one AlAs layer at the first interface (AlSb on InAs) should reinforce the natural tendency towards Al-As type interface and increase the tensile stress (negative out of plane strain), which is actually observed. At the second interface (InAs on AlSb), the addition of one AlAs layer should lead to the formation of a very high tensile interface, but the experimental analysis suggests a more moderate tensile stress, in agreement with the possible mixing of elements V suggested by the sequence analysis. On the contrary, the addition of one InSb monolayer at the first interface is clearly useless under these growth conditions, leading to a wide interface, with a moderate tensile stress. At the second interface the addition of one InSb monolayer produces a strong compressive stress, as expected; however an $Al_{0.5}In_{0.5}Sb$ rich interface is formed rather than InSb due to the unstable character of In-Sb bond.

In summary, Al-As type interfaces can be achieved easily during the MBE growth of InAs/AlSb multilayers, both on InAs and AlSb ; this can be explained by the very high thermal stability of AlAs. The formation of an In-Sb type interface is clearly more difficult due to segregation of both In and Sb elements and due to its unstable atomic bond. Special growth conditions have to be tried in order to stabilize the In-Sb type interface.

ACKNOWLEDGMENTS

The authors are grateful to C. Crestou for TEM samples thinning. The research leading to these results has received funding from the European Union Seventh Framework Programme under Grant Agreement 312483 - ESTEEM2 (Integrated Infrastructure Initiative–I3). This work is supported by the French national project NAIADE (ANR-11-BS10-017).

REFERENCES

[1]O. Cathabard, R. Teissier, J. Devenson, J. C. Moreno, and A. N. Baranov, Appl. Phys. Lett. 96, 141110 (2010).

[2]P. Laffaille, J. C. Moreno, R. Teissier, M. Bahriz, and A. N. Baranov, AIP Adv. 2, 022119 (2012).

[3]G. Tuttle, H. Kroemer and J. H. English, J. Appl. Phys. 67, 6 (1990).

[4]J. Spitzer, A. Hopner, M. Kuball, M. Cardona, B. Jenichen, H. Neuroth, B. Brarand and H. Kroemer, J. of Appl. Phys. 77 (2), 811 (1995).

[5]K. Mahalingam, H. J. Haugan, G. J. Brown, and K. G. Eyink, Ultramicroscopy 127, 70 (2013).

[6]J. H. Li, D. W. Stokes, O. Caha, S. L. Ammu, J. Bai, K. E. Basslerand and S. C. Moss, Physical Review Letters **95** (9), 096104 (2005).

7B. Z. Nosho, B. R. Bennett, L. J. Whitman and M. Goldenberg, Applied Physics Letters **81** (23), 4452 (2002).

[8]B. Satpati, J. B. Rodriguez, A. Trampert, E. Tournié, A. Joullié and P. Christol, Journal of Crystal Growth **301**, 889 (2007).

[9]E. Luna, F. Ishikawa, B. Satpati, J. B. Rodriguez, E. Tournié and A. Trampert, Journal Of Crystal Growth **311** (7), 1739 (2009).

[10]Y. Ashuach, Y. Kauffmann, C. Saguy, S. Grossman, O. Klin, E. Weiss and E. Zolotoyabko, J. of Appl. Phys. **113**, 184305 (2013).

[11]H. Kim, Y. Meng, J. L. Rouviere, D. Isheim, D. N. Seidman, and J. M.Zuo, J. Appl. Phys. 113, 103511 (2013).

[12]W. Barvosa-Carter, M. E. Twigg, M. J. Yang and L. J. Whitman, Phys. Rev. B **63**, **245311** (2001).

[13]A. Bauer, M. Dallner, A. Herrmann, T. Lehnhardt, M. Kamp, S. Höfling, L. Worschech and A. Forchel, Nanotechnology 21 (45),455603 (2010).

[14]B. Bonef, L. Gerard, J.-L. Rouviere, A. Grenier, P.-H. Jouneau, E. Bellet-Amalric, H. Mariette, Regis Andre and C. Bougerol, Appl. Phys. Lett. 106, 051904 (2015)

[15]J. Nicolaï, Ch. Gatel, B. Warot-Fonrose, R. Teissier, A.N. Baranov, C. Magen and A. Ponchet, Appl. Phys. Lett. 104, 031907 (2014).

[16]C.L. Jia, M. Lentzen and K. Urban, Science 299, 870 (2003).

[17]M. J. Hytch, E. Snoeck and R. Kilaas, Ultramicroscopy **74** (3), 131 (1998).

[18]E. J. Kirkland, Ultramicroscopy **23**, 77 (1987).

[19]S. J. Pennycook, Ultramicroscopy **30**, 58 (1989).

[20]C.T. Koch, PhD. thesis, Arizona State University, 2002.

[21]V. Swaminathan and A. T. Macrander, *Materials Aspects of GaAs and InP Based Structures* (Prentice-Hall. Inc., Englewood Cliffs, New Jersey, 1991) (ISBN 0-13-346826-7).

[22]L. Pedesseau, J. Even, A. Bondi, W. Guo, S. Richard, H. Folliot, C. Labbe, C. Cornet, O. dehaese, A. LeCorre, O. Durand and S. Loualiche, J. Phys. D: Appl. Phys. 41, 165505 (2008)

[23]F. Pailloux, M. L. David and L. Pizzagali, Micron **41**, 135 (2010).

[24]C. Gatel, H. Tang, C. Crestou, A. Ponchet, N. Bertru, F. Doré and H. Folliot, Acta Materialia **58** (9), 3238 (2010).

[25]I. Prévot, B. Vinter, X. Marcadet and J. Massies, Appl. Phys. Lett. **81** (18) 3362 (2002).

[26]G. B. Stringfellow, Journal of Crystal Growth **58**, 194 (1982).

[27]K. Ishida, T. Nomura, H. Tokunaga, H. Ohtani and T. Nishizawa, Journal of Less-Common Metals **155**, 193 (1989).

[28]A. N. Semenov, A. N. Semenov, V. A. Solov'ev, B. Ya. Meltser, Y. V. Terent'ev, L. G. Prokopova and S. V. Ivanov, Journal of Crystal Growth **278**, 203 (2005).

[29]R. Kaspi and K. R. Evans, Appl. Phys. Lett. **67** (6), 819 (1995).

[30]A. M. Sanchez, A. M. Beltran, R. Beanland, T. Ben, M. H. Gass, F. de la Peña, M. Walls, A. G. Taboada, J. M. Ripalda and S. I. Molina, Nanotechnology **21**, 145606 (2010).

[31]J. Massies, F. Turco, A. Saletes and J.P. Contour, Journal of Crystal Growth **80**, 2, (1987).

[32]C. T. Foxon, Journal of Vacuum Science & Technology B 1, **293** (1983).

Figure captions

FIG. 1. (Color on line) Growth sequence of the samples. (a) In the sample A the interfaces are spontaneously assembled. (b) In the sample B we tried to make AlAs then InSb interfaces while in the sample C (c) we tried to make InSb then AlAs interfaces.

FIG. 2. (Color on line) Schematic representation of the different types of interface between two systems, A and B, with no common atoms. (a) Minimal interface with a simple atomic bond between A and B layers. (b) Topological interface due to roughness, generally about one atomic layer in the semiconductor materials. (c) Chemical interface where the diffusion mechanisms (for miscible materials) result in an intermediate mixed layer.

FIG. 3. (Color on line) (a) Misfit f with InAs and (b) average atomic number Z, for the four possible ternary compounds. The horizontal dashed lines correspond to InAs and AlSb.

FIG. 4. Curves of (a) iso misfit with InAs substrate and (b) iso average Z versus chemical composition, for quaternary alloys.

FIG. 5. (Color on line) (a) HRTEM image of A sample [110] zone axis, (b) $\varepsilon_{\perp}$ mapping, (c) $\varepsilon_{\perp}$ strain profile obtain by GPA averaged on the whole width of the image (30 nm). The white arrow indicates the growth direction.

FIG. 6. (a) HAADF-STEM micrograph of sample A. The arrow indicates the growth direction. (b) Intensity profile of HAADF micrography, plotted along the growth direction. The intensity is given in arbitrary unit (the intensity variation between the different InAs layers is related to the thickness variation of the sample).

FIG. 7. Quaternary compounds composition from HRTEM and HAADF-STEM analysis.

FIG. 8. (Color on line) (a) $\varepsilon_{\perp}$ mapping of B sample, from GPA of an [110] zone axis HRTEM image, (b) $\varepsilon_{\perp}$ strain profile averaged on the whole width of the image (30 nm), (c) HAADF-STEM micrograph of sample B, (d) Intensity profile of this HAADF micrography plotted along the growth direction.

FIG. 9. (Color on line) (a) $\varepsilon_{\perp}$ mapping of C sample, from GPA analysis of an [110] zone axis HREM image, (b) $\varepsilon_{\perp}$ strain profile averaged on the whole width of the image (30 nm), (c) HAADF-STEM micrograph of sample C, (d) Intensity profile of the HAADF micrography, plotted along the growth direction.